

ECOLE POLYTECHNIQUE FÉDÉRALE DE LAUSANNE



Design, fabrication and control of an Origami Haptic Platform

Author:

Yves MARTIN

Professor:

Prof. Jaime PAIK

Supervisor:

Mustafa METE

A semester project at Reconfigurable Robotics Lab

August 30, 2023

Table of contents

| | |
|--|-----------|
| 1 Abstract | 3 |
| 2 Introduction | 4 |
| 2.1 Motivation | 5 |
| 2.2 State of the art | 6 |
| 2.3 Main contributions | 7 |
| 2.4 Two different prototypes | 7 |
| 3 Design and fabrication of the origami-based 3-DOF fully rotational structure "Double Waterbomb" | 9 |
| 3.1 Layers design | 9 |
| 3.1.1 Avoid misalignments with a good design | 10 |
| 3.1.2 Optimal hinge-width characterization | 10 |
| 3.1.3 How to keep origami standing up straight at rest position | 11 |
| 3.2 Material used and fabrication | 12 |
| 3.2.1 Material used | 12 |
| 3.2.2 Fabrication | 12 |
| 4 Characterization | 14 |
| 4.1 Characterization in torque of the DW | 14 |
| 4.1.1 Choices and assumptions | 14 |
| 4.1.2 Two consecutive setups | 14 |
| 4.2 Results | 16 |
| 4.3 Safe range of external torque to apply on DW characterization | 18 |
| 5 Empirical modeling | 19 |
| 5.1 Definitions | 19 |
| 5.2 Sub-systems modeling | 20 |
| 5.3 The roll sub-model | 21 |
| 5.4 The pitch sub-model | 21 |
| 5.5 The yaw sub-model | 22 |
| 5.6 Fit and plots of the sub-models | 22 |
| 5.6.1 Fitting the sub-models | 22 |
| 5.6.2 Comparing symmetric joints to challenge the results | 22 |
| 5.7 Getting the kinematics model by putting sub-models together | 23 |
| 5.7.1 The gimbal kinematic model | 23 |
| 5.7.2 The 3-DOF fully rotational kinematic model | 23 |
| 5.8 How to avoid tracking an impossible \vec{d} | 25 |
| 5.9 Figures | 26 |

| | |
|--|-----------|
| 6 1st project : sensing and actuation for a rotary pouch motors actuated design | 32 |
| 6.1 Sensing | 32 |
| 6.1.1 Sensors selection | 32 |
| 6.1.2 Sensing design | 32 |
| 6.1.3 Sensors reading using I ² C | 33 |
| 6.2 Actuation | 34 |
| 6.2.1 Stacking pouches to propose a different type of Rotary Pouch Actuator than Adibnazai and al., 2020 | 35 |
| 6.2.2 Pouch motors are a good option for origami-based VR controller | 36 |
| 6.2.3 Why Pouch motors were not implemented in DW ? | 36 |
| 7 2nd project: DC-motor integration and control | 37 |
| 7.1 Motor selection | 37 |
| 7.2 Design | 37 |
| 7.3 Hardware and software setups | 38 |
| 7.4 Control in position | 39 |
| 8 Discussion | 40 |
| 8.1 Design improvement advantages | 40 |
| 8.2 A simple model for high performances and popular use | 40 |
| 8.3 Using Pouch motors asymmetry to implement haptics | 41 |
| 8.4 DC-motor control position is accurate, but not adapted to haptic | 42 |
| 9 Conclusion | 43 |
| 10 Bibliography | 44 |

1 Abstract

This report is the end result of a semester project performed by Yves Martin at Reconfigurable Robotics Lab.

In order to develop an origami-based haptic platform, this project focused on the design, the characterization, the actuation and the control of a "Double Waterbomb" (DW) origami. The current State-of-the-Art was explored and is summarized below. Several prototypes of DW were designed and machined. Design challenges were solved, such as having the DW standing up straight at rest, avoiding parasites movements, and avoiding misalignment. A characterization setup was developed, and the DW was characterized. An empirical kinematic model was made, linking joystick position to bottom-hinges angles. The possibility to use stacked rotary pouches as actuators was explored but not implemented, due to issues with folding. Sensing for DW hinges angles was implemented, including sensor selection, integration on the platform, and reading from the computer. DC motors were selected and integrated to the platform as actuators. Position control was implemented.

2 Introduction

This section will introduce the main ideas of the project. First, an overview of what robogamis are will be shown. Then, the motivation of the project will be exposed. Eventually, a brief statement of the current State-of-the-Art will be made.

Origami-inspired⁽¹⁾ structures idea started in the 2000's. They are an opportunity to create fast, light-weight and low-cost fabrication robots. Combined "robogamis" can perform high-DOF kinematic structures. Robogamis are versatile tools for low-tech and high tech applications, such as worm-robots⁽²⁾ or teleoperated microsurgery manipulators⁽³⁾.

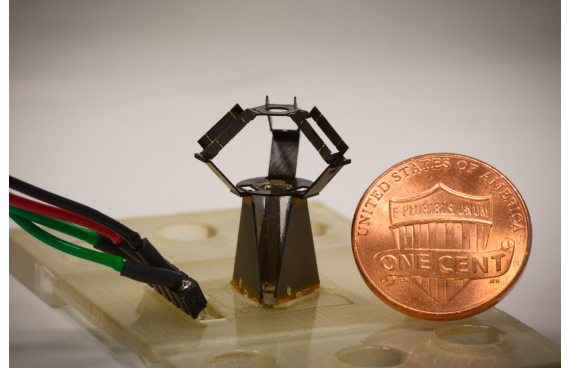


Figure 2.1: Light-weight milliDelta robogami can get up to 35Hz, Suzuki and al. 2020⁽³⁾

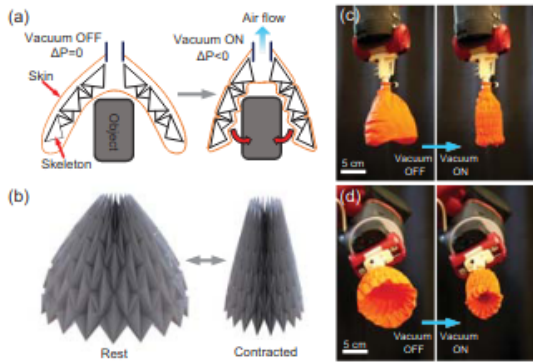


Figure 2.2: An example of an actuated high-DOF kinematic structure: vacuum-actuated robogami, Li and al. 2019⁽⁴⁾

Origami-based structures can constraint any geometry⁽⁵⁾. One of the challenges of the roborigami creation are then the actuation of each origami-based structure, in order to turn a constraining structure into a controllable robot. Many researches have been made on the different ways of actuating the origami-based structures. Vacuum driven⁽⁴⁾, using shape-memory composites⁽⁶⁾, pneumatic pouches, piezoelectric materials, shape memory alloys, electric motors⁽⁷⁾, etc.

On one hand, origami-based structures are an innovative way to create light-weight, low-cost and various kinematic structures. On the other hand, actuated spherical joints are still a challenge to design using more traditional design methods. The realization of an actuated origami-based spherical joint would open opportunities for the industry.

2.1 Motivation

Virtual-Reality (VR) controllers are an opportunity to use origami-based spherical joints. They need to be light-weight to be worn, and having them low-cost is a real plus to be able to scale up their production. They need to be actuated in order to implement haptic control, to give the user a more immersive VR experience. VR controllers could be a good proof of concept of the feasibility, desirability and viability of origami-based spherical joints.

Pouch motors are lightweight and high-strength. It is typically lighter than electric actuation. As the origami-based structures are also lightweight, pneumagamis are an opportunity to create lightweight robots, for instance for wearable robotics, as proposed by Robertson and al. (2021). Implementing haptic control over the top would for instance open opportunities for wearable VR equipment, allowing the player to send and receive sensation from the game by the pouch pressure. This would enhance the VR user-experience with one more sense, the touch, like 5D cinema.

A first step towards an origami-based VR controller would be to build a Virtual-Environment (VE) interface. This interface includes an origami-based pouch-actuated haptic platform (i.e the controller itself), and a VE to connect it. Eventually, the DW was actuated with DC motors.

This project was lead by Mustafa Mete. The VE development of the project was taken care of by Bruno Trivelli, and the origami-based haptic platform part was taken care of by Yves Martin.

2.2 State of the art

Rotary pouch actuators⁽⁸⁾ can control millimeter-scale 1-DOF joint. The idea of using pouch motors to control origami-based robots is not new: Robertson and al. implemented in 2020 pouch SPAs on a "pneumagami"⁽⁹⁾ module in order to reach lightweight, high-strength, and compact pneumagami modules. Moreover, haptic control has already been achieved using soft-pneumatic actuator⁽¹⁰⁾. This project aimed to combine both ideas, developing a haptic origami-based platform with rotary pouch motors.

One of the issue with pneumagamis is that rotary pouch actuators cannot reach more than 60° of angular range. Another issue is that at the moment, there is no characterization of the pressure to force relationship in pouch motors, which makes the control harder.

The control of origami robots includes joint angle control and coordination of the various joint actuators. In general, the control is made by joint control, external folding or self-folding⁽⁷⁾. A framework for interacting with robotic origamis⁽¹¹⁾ in a virtual environment by providing intuitive control methodology was developed by Huang and al., 2018. Huang's method inspired this project, which aims to implement haptics control.

As explained in the motivation, the initial project was to build a Haptic platform using rotational pouch motors. This doesn't existe in the State-of-the-Art yet, but it is across many previous researches. Haptic control had already been implemented using SPAs⁽¹⁰⁾ (Sonar and al.). Rotational pouch motors⁽⁸⁾, proposed by Adibnazai and al.(2020), had also already been implemented on origami-based structure and nicknamed "pneumagami"⁽⁹⁾ (Robertson and al. 2021), but without implementing a haptic control.

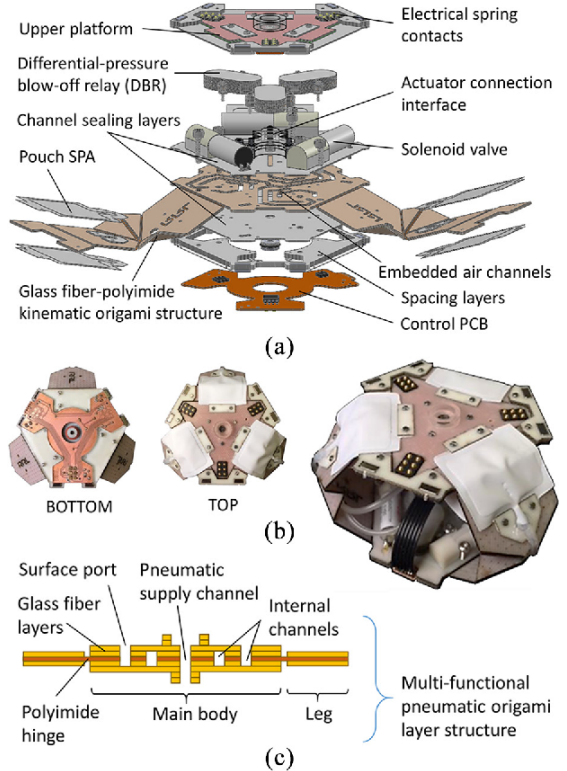


Figure 2.3: A pouch-actuated robogami: Robertson and al. "Pneumagami"⁽⁹⁾

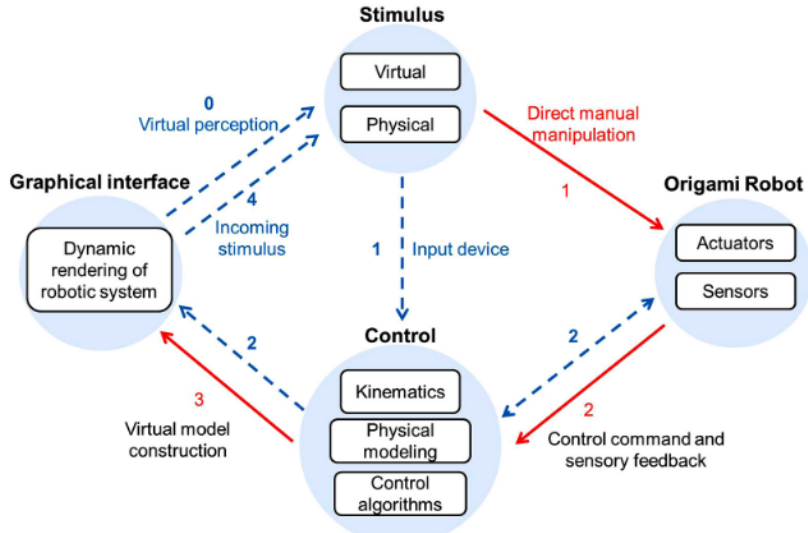


Figure 2.4: Huang and al. control methodology⁽¹¹⁾

2.3 Main contributions

The main contributions of this project are:

- Enhancing the "Double-WaterBomb" (DW) design, DW being two Waterbomb origami-based 2D structures put in serial (see fig. 2.5 and 2.6)
- Developing a 3-DOF fully rotational kinematic torque characterization DW setup and using it to characterize in torque the stiffness of the DW
- Proposing an empirical forward kinematic model for the DW
- Integrating Hall-effect sensors on origami-based structure
- Exploring the use of stacked rotary pouch actuators combined with Hall-effect sensors for robogami
- Implementing position control on a DW using DC-motors and encoders integrated to the platform

2.4 Two different prototypes

The project was initially to actuate a DW with pouch motors, then to actuate DW with DC-motors. Therefore, two prototypes were produced. This report will cover both projects. The two prototypes are shown below.

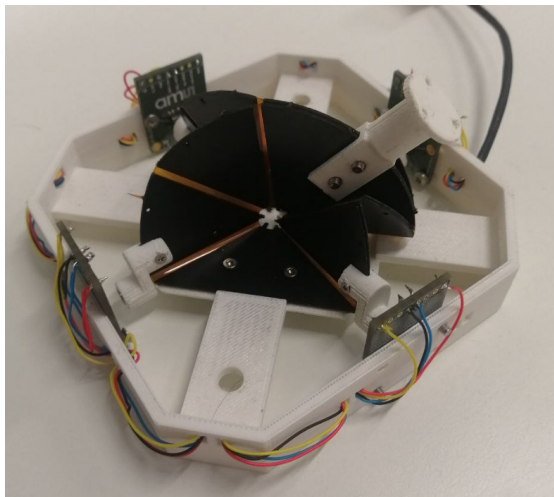


Figure 2.5: 1st prototype, to implement pouch actuation and using Hall-effect sensors

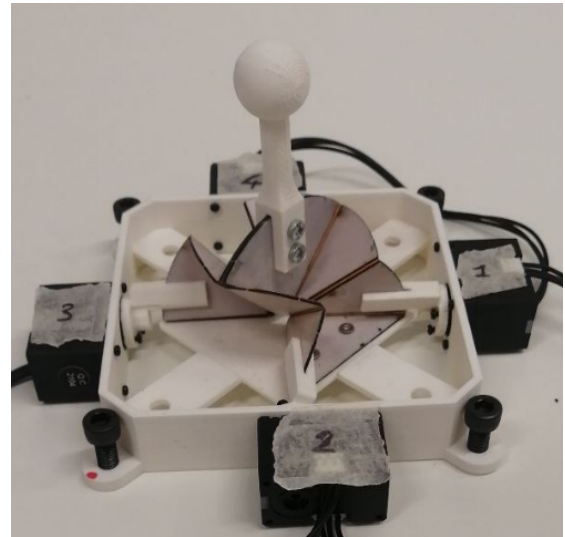


Figure 2.6: 2nd prototype, using DC-motors and encoders

3 Design and fabrication of the origami-based 3-DOF fully rotational structure "Double Water-bomb"

The Double-Waterbomb (DW) is an origami-based spherical joint structure. The degrees of freedom are all rotational and will be called roll, pitch, yaw. As any origami-based structure, the DW is a 3D structure folded from a 2D sheet. The DW is controllable from its 4 bottom hinges. A photo of a DW sample screwed on a 3D printed base is shown on fig. 3.1.

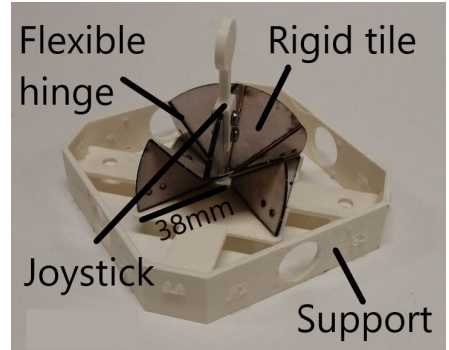


Figure 3.1: Prototype of the DW robogami platform without the motors

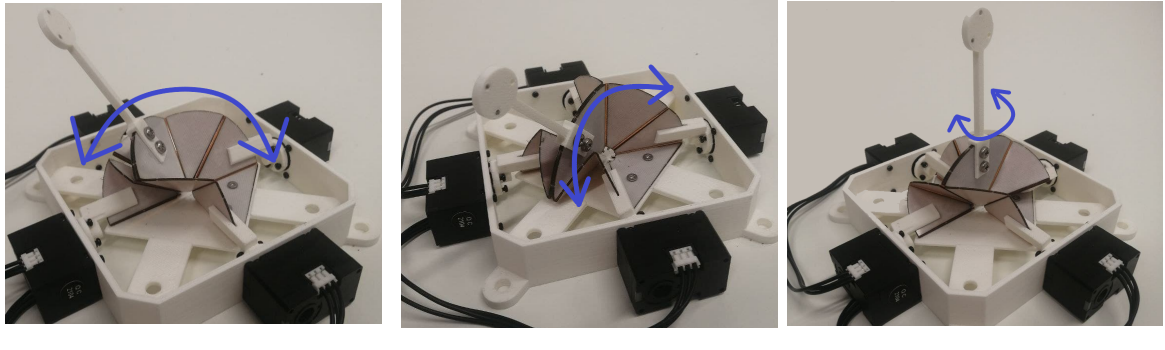


Figure 3.2: DW rotating through its 3 axis

3.1 Layers design

The design of the structure consists in drawing in 2D the Waterbombs, in order to fold them into a 3D structure afterwards. Fusion 360, a mechanical design software, was used to design the DW. The plans are on the fig. 3.3. As one can see on the plans, the FR4 and the adhesive are cut at the hinges such that they are cut into tiles. The Kapton stays in one part. There is holes to fix the DW on the platform, and the Hall-effect sensors / DC motors on the origami.

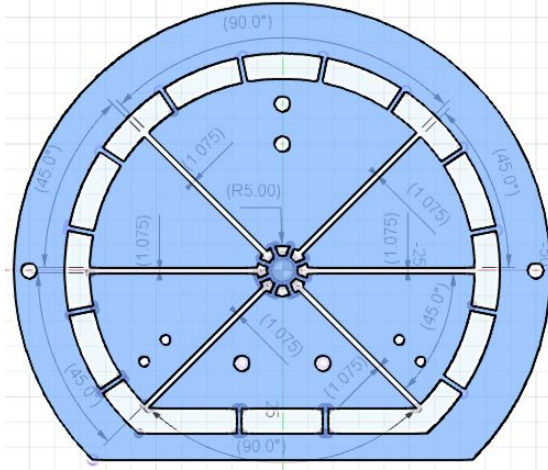


Figure 3.3: Design of FR4 layers and adhesive layers for Waterbomb origami-based structure

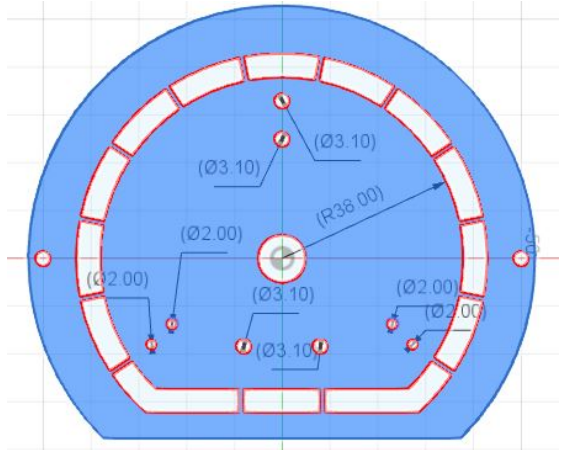


Figure 3.4: Design of Kapton layer for Waterbomb origami-based structure

3.1.1 Avoid misalignments with a good design

One of the main issues when fabricating a FR4/adhesive/Kapton/adhesive/FR4 sandwich is that misalignment occur easily, especially as the adhesive melts during heating and as the sample is under pressure. This is why the design integrates holes for alignment (cf part 3.2.2), such that each layer stay aligned by each other during heating. Also, within the adhesive and FR4 layer, misalignment of tiles relatively to the other tiles can occur. This is why all tiles are held together by two circles, one all around the sample and one inside, that connects to every tiles with 1mm links. That way, each tile is held by 3 links, and no misalignment occurs.

3.1.2 Optimal hinge-width characterization

The hinge width, i.e the width between two tiles, is crucial in the DW design. When fabricating a first draft DW sample, an issue occurred as the hinge width was too large, and therefore the rotational axis of the hinges has parasites movements. This was an issue, especially as the AS5048 Hall-effect sensors, used on the pouch-actuated prototype, tolerate 0.25mm of misalignment according to its datasheet. But, if the hinge-width is too small, the origami can't fold. Therefore, a trade-off has to be found to select the best hinge width.

In order to select the best hinge width possible for given dimension of Kapton and FR4, the sample shown on fig 3.7 was produced. 6 hinges were produced, with the following hinge width values:

$$W_{hinge} = W_{Kapton} + 2W_{FR4} + 2W_{Adhesive} + \epsilon \quad (3.1)$$

$$\left| \begin{array}{l} \epsilon = \{0.1, 0.2, 0.3, 0.4, 0.5, 0.6\} \text{mm} \\ W_{Kapton} = 125 \mu\text{m} \\ W_{FR4} = 0.3 \text{mm} \\ W_{Adhesive} = 25 \mu\text{m} \end{array} \right.$$

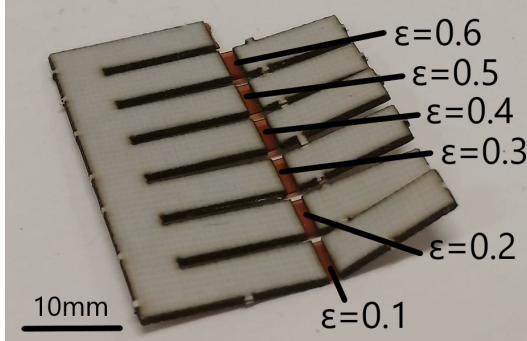


Figure 3.5: Sample for characterization of the joint width. The width are sorted by size, the smallest on the front and the largest on the back.

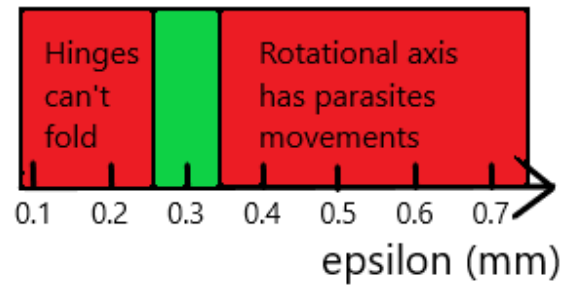


Figure 3.6: The joint-with trade-off

As a result of this experiment, $\epsilon=0.3 \text{mm}$ was selected.

3.1.3 How to keep origami standing up straight at rest position

When the first DW prototype was produced, it didn't stand up straight and would use (0 deg, 20 deg, 0 deg) as rest position. Also, the prototype would easily get into singularities. In order to get rest position at (0 deg, 0 deg, 0 deg), and to avoid getting the DW into singularities, the following process was applied:

- Increase the Kapton thickness from 75 μm to 125 μm
- Reduce the hinge width epsilon from 0.75mm to 0.3mm (cf 3.5)
- Give each Waterbomb hinge shape memory by folding, heating then cooling them down

3.2 Material used and fabrication

3.2.1 Material used

An origami is made of rigid tiles and flexible hinges. To fabricate the tiles of the origami-based structure, a type of glass-reinforced epoxy laminate material called FR4 by a NEMA designation is used. Hinges are made out of Kapton, a film of polyimide (high performance plastics). To assemble hinges and tiles, a "sandwich" of FR4 is made, with Kapton in the middle. FR4 and Kapton are held together by adhesive.

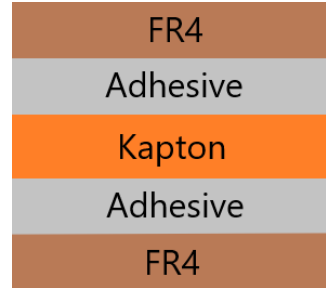


Figure 3.7: Material used

The range of typical width for FR4 would be 0.2mm to 1mm, and the range of typical width for Kapton would be $25\mu\text{m}$ to $150\mu\text{m}$. Two DW samples were produced. The sample produced to implement pouch motors was produced with $75\mu\text{m}$ Kapton. The characterization of this sample showed a weak range of torques. This is an issue, because then the origami gets easily into singularity positions. In order to increase the stiffness, the DC motor driven sample was produced using $125\mu\text{m}$ Kapton. A log of the material dimensions is on tab 1.

Samples of simple hinges fabricated with FR4 and Kapton are shown on fig. 3.5.

| | Kapton | FR4 | Adhesive |
|------------------------|------------------|-------|-----------------|
| Pouch Sample | $75\mu\text{m}$ | 0.5mm | $25\mu\text{m}$ |
| DC motor driven sample | $125\mu\text{m}$ | 0.3mm | $25\mu\text{m}$ |

Table 1: Dimension of the material used

3.2.2 Fabrication

To assemble all of the material, metal plates with alignment pins holes are used. On those plates, the distance between two adjacent alignment pin holes is 25mm, and the diameter of the pin holes is 3.10mm. Samples are aligned on those plates with alignment pins, as shown on fig.3.8.

Then, the sample is covered with another metal plate and heated at 130°C under a pressure of 60 psi. Once this cooking done, it is advised to let the sample cool down during a few minutes before touching it after the heating, to avoid getting misalignments. Eventually, the sample is ready.

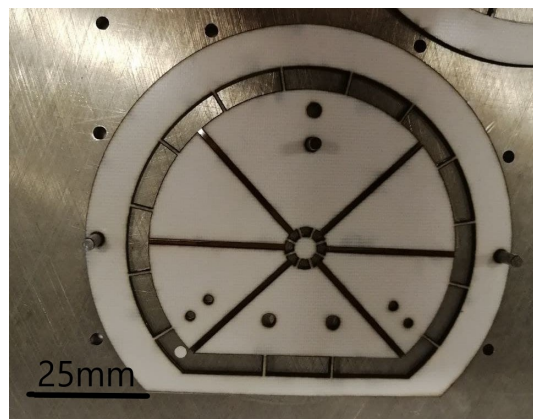


Figure 3.8: Alignment of the sample on a metal plate

4 Characterization

This part covers the characterization of the DW's stiffness in torque, using a 3-DOF fully rotational kinematic torque setup. It also gives a safe range of external torques to apply on the DW.

4.1 Characterization in torque of the DW

4.1.1 Choices and assumptions

Only the DC-motor driven sample was characterized, because the pouch sample was not very stiff. Also, in order to know the variance of the measurement, each sample were characterized 5 times, and the standard deviation is shown on the graphs. The angular sample resolution is 5° , as the measured values didn't change much within 5° . To measure with precision the hysteresis due to plastic deformation, the measurements are made alternatively in a direction, then in the other direction.

Each DOF (roll, pitch, yaw) was characterized separately, the others DOF being at rest point (i.e 0) meanwhile. This is because the overall range of possibilities of DW structure configuration is the product of the ranges of roll, pitch and yaw, which are shown in tab. 4.1. To measure absolutely all configurations, using a resolution of 0.1 rad ($\sim 5.7^\circ$), and taking 5 measures per configuration, it would take 16'875 measurements. This is possible but requires an appropriate setup.

It is supposed that the characterization setup induces no friction. The force/torque (F/T) sensor used is a 6-axis F/T Nano-17, read by a Labview code. In the first place, it was supposed that there was no hysteresis, i.e that the position of the joystick would be the only factor determining the resulting moment. This assumption wasn't true, as shown in the results, and therefore removed.

4.1.2 Two consecutive setups

A first setup was built to characterize the sphere. This setup gave bad results, because the force sensor was hold with the hand. This is why a second setup was built.

FIRST SETUP

In order to characterize the sample right along each axis, a characterization sphere was 3D printed with a linear track. It is guiding a joystick fixed upon the top of the Waterbomb structure. The track is covered with teflon in order to limit the dry friction

| | |
|-------|------------------------------------|
| Roll | $[-\frac{\pi}{2}, \frac{-\pi}{2}]$ |
| Pitch | $[-\frac{\pi}{4}, \frac{-\pi}{4}]$ |
| Yaw | $[-\frac{\pi}{4}, \frac{-\pi}{4}]$ |

Figure 4.1: Ranges of the DW kinematic

of the track with the joystick. For roll (resp. pitch), the joystick is 3.3mm large, which is enough to keep the joystick at 0° on pitch (resp. roll) and yaw. It is also large enough to have no dry friction. In order to measure the force, the sensor was pushed with the hand to the desired position. See fig. 4.4.

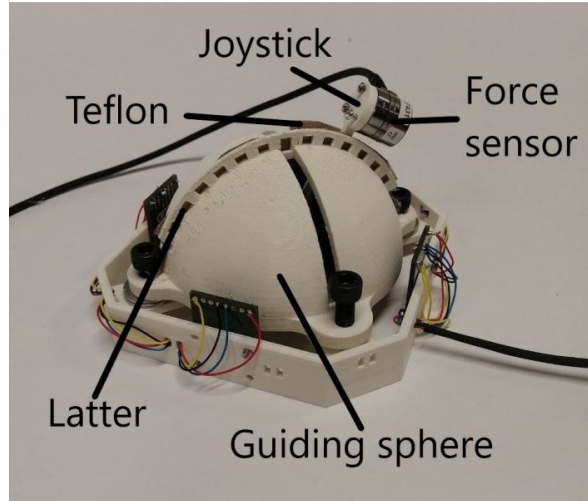


Figure 4.2: First setup used for the characterization

In order to characterize 3 axis, 3 joysticks were 3D printed, see fig. 4.3. It was necessary to print 3 joysticks for the following reasons. For roll and pitch, to measure the torque as a force normally applied on the force sensor along the axis with the sensor. For yaw, the torque is measured using the z-axis torque sensor of the F/T sensor.

To associate the measured value with an angle configuration, one can see on fig. 4.4 that a latter is part of the characterization sphere such that, by aligning the joystick with the latter, it is possible to read precisely the angle.

This setup gave inconsistent and noisy results, because hand-hold measurement is not precise enough. This is why a second setup was built, avoiding this problem.

SECOND SETUP

The operating principle of the second setup is the same as the first one, except that instead of holding the joystick directly with the hand, it is hold with a guide.

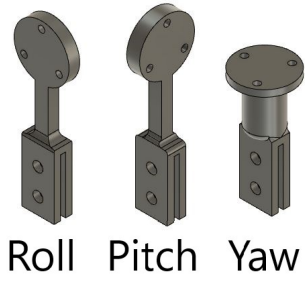


Figure 4.3: Joysticks used for characterization

Teflon was removed, as the track reference of the guiding sphere isn't touching the joystick anyway, it is only a sanity check that the joystick stays in the right axis.

This setup gave the results shown in part 4.2.

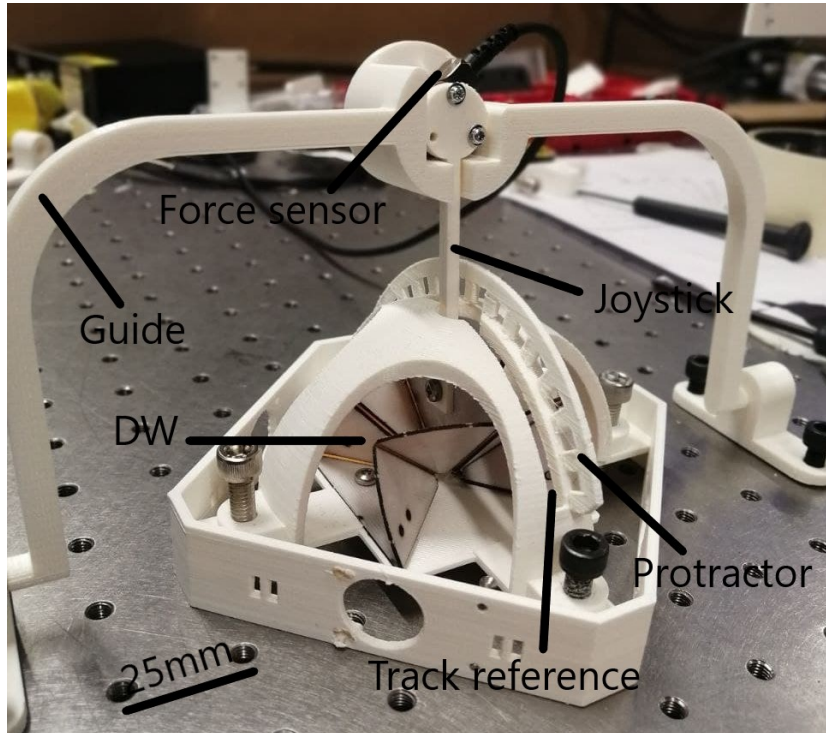


Figure 4.4: Second setup used for the characterization

4.2 Results

Due to the plastic deformation of the Kapton layer, the restoring force of the sample is an hysteresis. This is why measurements are made forward, then backwards, and so on 5 times. One can see that have the same behavior:

- Spring behavior in a certain range of motion around the origin with torque constants of K_{Roll} , K_{Pitch} and K_{Yaw} . K_{Pitch} is surprisingly negative, almost zero.
- Increasing torque - over-passing the spring behavior - when pushing the DW to its extrema.
- Plastic deformation when pushing the DW in a direction, adding a T_{off} component to the equation, which means an hysterical behavior

$$T_{axis}(\theta_k) = -K_{axis}(\theta_k - \theta_{axis}^0) + T_{off}(\vec{\theta}) \quad (4.1)$$

For a given axis:
 T_{axis} is the torque
 K_{axis} is the torque constant
 θ_k is the current angle
 θ_{axis}^0 is the rest point
 $T_{off}(\vec{\theta})$ is the offset torque due to plastic deformation, deductible from previous positions

Figure 4.5: Model of the DW behavior around the origin

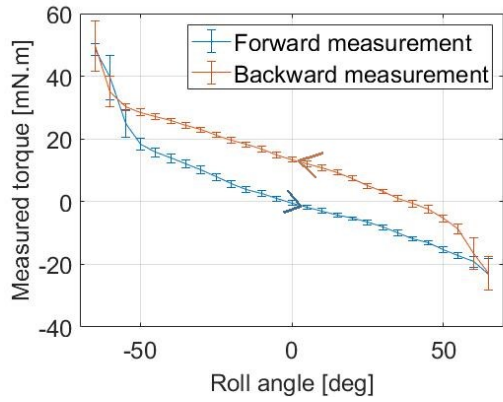


Figure 4.6: Torque characterization of the DW stiffness along roll(θ)

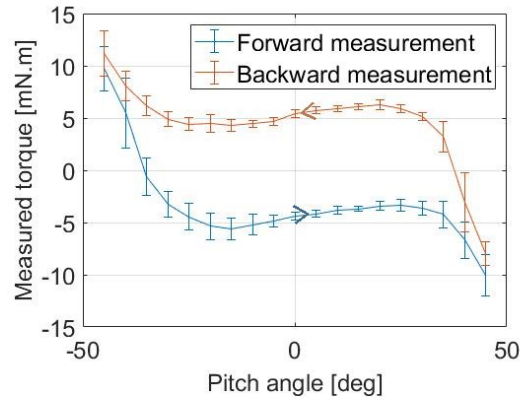


Figure 4.7: Torque characterization of the DW stiffness along pitch(ϕ)

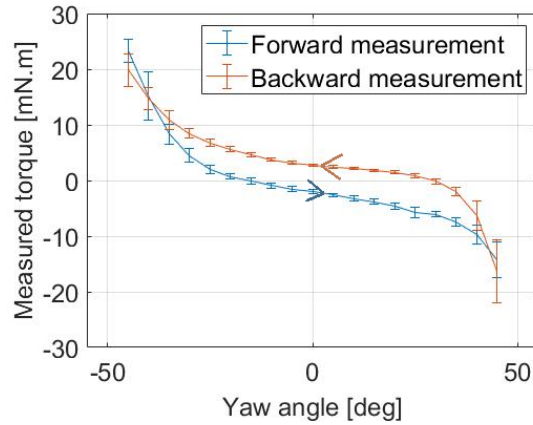


Figure 4.8: Torque characterization of the DW stiffness along yaw(γ)

4.3 Safe range of external torque to apply on DW characterization

To give an idea of what torque can be externally applied on the DW along the different axis without damaging the sample, measurements have been done. The same was stuck in rest position (vertical) by the bottom hinges. The force sensor was manually applied on the sample to measure how much force could be put in. These values are not maximal safe values, but indicate a safe zone of torque to apply on the DW.

| Axis | Maximum measured value |
|-------|------------------------|
| Roll | 0.08 [N.m] |
| Pitch | 0.09 [N.m] |
| Yaw | 0.5 [N.m] |

Table 2: Safe range of external torque to apply on DW characterization

5 Empirical modeling

In this section will be proposed a kinematic model for the DW. This model links the bottom-hinges angles and the joystick position. This model is empirical, which means it is based on observations, instead of theory or simulation. The angles of the DW have been measured, using the DC-motors encoders on the motor actuated prototype, and fitted to polynoms. It gave the following kinematic model. The positions of motors 1, 2, 3, 4, corresponding to joints q_1 , q_2 , q_3 , q_4 , are shown on fig. 5.1, with q_4 as an example.

This model should be challenged with experiments and theory to be considered as reliable. Thought, first observations shows that this model present great results.

This project is an opening for inverting the following kinematic model.

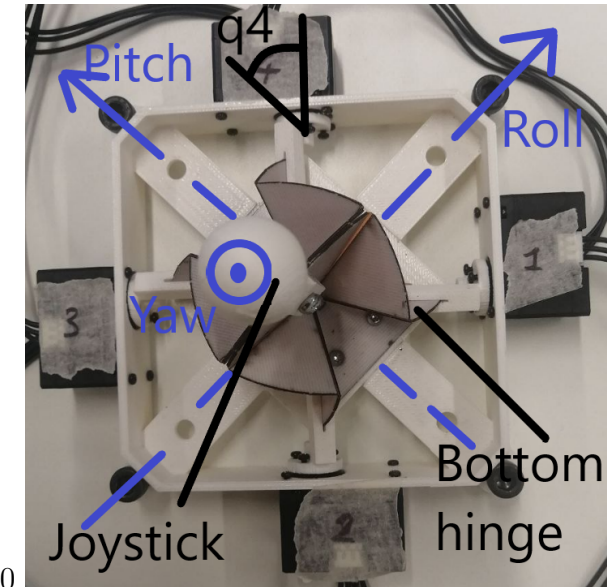


Figure 5.1: DC-motors with encoders platform, showing the rotational axis, identifying the joint q_4 , the joystick and a bottom hinge

5.1 Definitions

Let's define several useful terms.

The **roll** axis is shown on fig 3.2. Its corresponding angle is θ . This axis is defined with respect to the platform, it doesn't change with the yaw angle of the DW.

The **pitch** axis is shown on fig 3.2. Its corresponding angle is ϕ . This axis is defined with respect to the platform, it doesn't change with the yaw angle of the DW.

The **yaw** axis is shown on fig 3.2. Its corresponding angle is γ .

The **axis** of the joystick is \vec{d} . It is written with Euler angles, such that:

$$\vec{d} = \begin{pmatrix} \theta \\ \phi \\ \gamma \end{pmatrix} \quad (5.1)$$

The **joints vector**, containing the joints angles, is \vec{q} , such that:

$$\vec{q} = \begin{pmatrix} q_1 \\ q_2 \\ q_3 \\ q_4 \end{pmatrix} \quad (5.2)$$

The unit is the degree. $\vec{q} = \vec{0}$ when every joint angle is forming a right angle with the platform plan. *Nota bene*, this is purely a theoretical reference for joints angles, $\vec{q} = \vec{0}$ cannot be reached by the DW.

The **kinematic model** is $\vec{\mathcal{F}}$ such that:

$$\vec{\mathcal{F}}(\vec{d}) = \vec{q} \quad (5.3)$$

The **inverse kinematic model** is $\vec{\mathcal{F}}^{-1}$ such that:

$$\vec{\mathcal{F}}^{-1}(\vec{q}) = \vec{d} \quad (5.4)$$

5.2 Sub-systems modeling

In the first place, each Euler angle, i.e each component of the \vec{d} vector, was modeled as an independent sub-system, setting the other Euler angles to zero. This gave the following equations.

The roll sub-model:

$$\vec{\mathcal{F}} \begin{pmatrix} \theta \\ 0 \\ 0 \end{pmatrix} = \vec{\mathcal{F}}_\theta(\theta) = \vec{q} \quad (5.5)$$

where \vec{q} slides on the roll axis.

The pitch sub-model:

$$\vec{\mathcal{F}} \begin{pmatrix} 0 \\ \phi \\ 0 \end{pmatrix} = \vec{\mathcal{F}}_\phi(\phi) = \vec{q} \quad (5.6)$$

where \vec{q} slides on the pitch axis.

The yaw sub-model:

$$\vec{\mathcal{F}} \begin{pmatrix} 0 \\ 0 \\ \gamma \end{pmatrix} = \vec{\mathcal{F}}_\gamma(\gamma) = \vec{q} \quad (5.7)$$

where \vec{q} slides on the yaw axis.

5.3 The roll sub-model

As mentioned above, this sub-system have to find a model such that:

$$\vec{\mathcal{F}}_\theta(\theta) = \vec{q} \quad (5.8)$$

where \vec{q} slides on the roll axis.

$$\vec{r}_2\theta^2 + \vec{r}_1\theta + \vec{r}_0 = \vec{q} \quad (5.9)$$

Using measurements of \vec{q} in function of \vec{d} , the following model is found:

The measurement fits pour each q_i are shown on fig. 5.4. The graphs comparing each joint to its adjacent joints are shown on fig. 5.5.

5.4 The pitch sub-model

As mentioned above, this sub-system have to find a model such that:

$$\vec{\mathcal{F}}_\phi(\phi) = \vec{q} \quad (5.10)$$

where \vec{q} slides on the pitch axis.

Using measurements of \vec{q} in function of \vec{d} , the following model is found:

$$\vec{p}_2\phi^2 + \vec{p}_1\phi + \vec{p}_0 = \vec{q} \quad (5.11)$$

The measurement fits pour each q_i are shown on fig. 5.6. The graphs comparing each joint to its adjacent joints are shown on fig. 5.7.

5.5 The yaw sub-model

As mentioned above, this sub-system have to find a model such that:

$$\vec{\mathcal{F}}_\gamma(\gamma) = \vec{q} \quad (5.12)$$

where \vec{q} slides on the roll axis.

Using measurements of \vec{q} in function of \vec{d} , the following model is found:

$$\vec{y}_1\gamma + \vec{y}_0 = \vec{q} \quad (5.13)$$

The measurement fits pour each q_i are shown on fig. 5.8. The graphs comparing each joint to its adjacent joints are shown on fig. 5.9.

5.6 Fit and plots of the sub-models

In this subsection will be covered the fit of the model to the measured data. Two types of plots are shown here. First, the fit of each sub-model to the measurement, made using the same setup as for the characterization. Second, for a given sub-model, the fit of the sub-model for a specific joint vs its adjacent joint. Each axis present those two plots.

5.6.1 Fitting the sub-models

The polynoms coefficients of each sub-models joints are computed using the mean-square algorithm to fit the measured data on a polynom along the corresponding axis (roll, pitch, yaw). This is shown on the first type of plot. It present surprisingly accurate results when looking at the complexity of the kinematics and the simplicity of the model. In fig 5.4, 5.6 and 5.8 are shown the fits.

5.6.2 Comparing symmetric joints to challenge the results

The second plot is interesting because the DW presents double symmetry. Thus, adjacent plots may be similar, 2-by-2. For instance, for the pitch sub-model, q_1 and q_4 are symmetric with respect to the pitch axis, and q_2 and q_3 as well. For the yaw sub-model, all joints are symmetric to the others with respect to the yaw axis.

Plotting a fit versus another fit that is supposed to be symmetric allows to challenge the results. As symmetric joints plots show lines, one can infer that the model seems accurate.

5.7 Getting the kinematics model by putting sub-models together

As explained on eq. 5.3, the kinematic model is $\vec{\mathcal{F}}$ such that:

$$\vec{\mathcal{F}}(\vec{d}) = \vec{q}$$

In order to make the merge of the sub-models as clear as possible, this subsection is organized in two parts. First will be shown the 2-DOF gimbal model, that combines roll and pitch control, with $\gamma=0$. Then, the 3-DOF fully rotational kinematic model will be exposed.

5.7.1 The gimbal kinematic model

The following hypothesis is made: the gimbal kinematic model is a linear function of the roll and pitch axis sub-models. To make an analogy with the electronic theory, this could be called the superposition theorem. Roll and pitch are independently controlled, and their merge gives the resulting model. This was not demonstrated, but only verified by experimentation.

$$\vec{\mathcal{F}} \begin{pmatrix} \theta \\ \phi \\ 0 \end{pmatrix} = \vec{\mathcal{F}}_\theta(\theta) + \vec{\mathcal{F}}_\phi(\phi) - \vec{C} \quad (5.14)$$

where \vec{C} is a constant vector called the rest position, such that

$$\vec{C} = \vec{\mathcal{F}}_\theta(0) = \vec{\mathcal{F}}_\phi(0) = \vec{\mathcal{F}}_\gamma(0) = \vec{\mathcal{F}} \begin{pmatrix} 0 \\ 0 \\ 0 \end{pmatrix} \quad (5.15)$$

5.7.2 The 3-DOF fully rotational kinematic model

The roll and pitch subsystems are computed with respect to the DW, and therefore sensible to its yaw orientation. But, the roll and pitch axis are defined with respect to the platform axis, i.e to the DW when $\gamma = 0$. It means that when $\gamma \neq 0$, roll or pitch movements are shifted by a γ angle on the yaw axis with respect to the platform roll and pitch axis. To correct this shift, a referential change have to be made to match the roll and pitch platform axis.

This γ dependence and the yaw axis control is integrated to the gimbal model (eq. 5.14). It gives the following model. It is validated by experimentation.

To change the unit vector's basis from the DW referential to the platform referential, one has to define new roll and pitch angles θ' and ϕ' to feed to the sub-models. Algebraically, this is a base change.

$$\theta' = \cos(\gamma)\theta + \sin(\gamma)\phi \quad (5.16)$$

$$\phi' = \sin(\gamma)\theta + \cos(\gamma)\phi \quad (5.17)$$

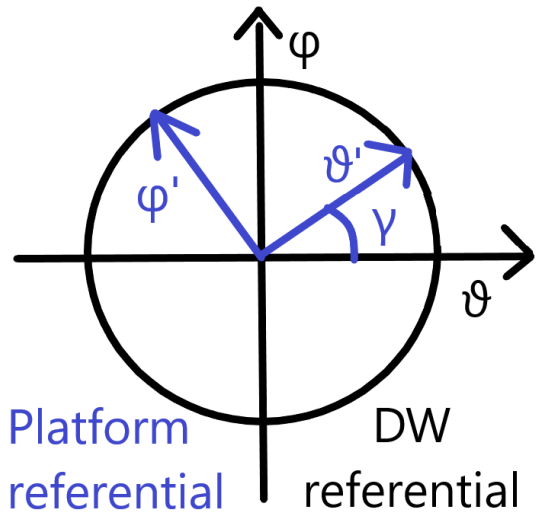


Figure 5.2: Roll and pitch referential change from the DW referential to the platform referential

$$\vec{\mathcal{F}} \begin{pmatrix} \theta \\ \phi \\ \gamma \end{pmatrix} = \vec{\mathcal{F}}_\theta(\theta') + \vec{\mathcal{F}}_\phi(\phi') + \vec{\mathcal{F}}_\gamma(\gamma) - 2\vec{C} \quad (5.18)$$

5.8 How to avoid tracking an impossible \vec{d}

When the other axis are set to zero, the theoretical range of motion along the roll, pitch and yaw axis are shown on fig 5.3. Though, the geometry of the DW makes that the range of motion along an axis depends on the other angles values.

| | |
|-------|------------------------------------|
| Roll | $[-\frac{\pi}{2}, \frac{-\pi}{2}]$ |
| Pitch | $[-\frac{\pi}{4}, \frac{-\pi}{4}]$ |
| Yaw | $[-\frac{\pi}{4}, \frac{-\pi}{4}]$ |

Figure 5.3: Ranges of the DW kinematic

This can be an issue, because while commanding the joystick in position, the user could ask for impossible position. It is easy to handle that issue with the kinematic model. As the model outputs target positions for \vec{q} , a simple check that every $q_i \in [q_{min,i}, q_{max,i}]$, $i \in \{1, 2, 3, 4\}$, with \vec{q}_{min} and \vec{q}_{max} measured on the real DW sample.

5.9 Figures

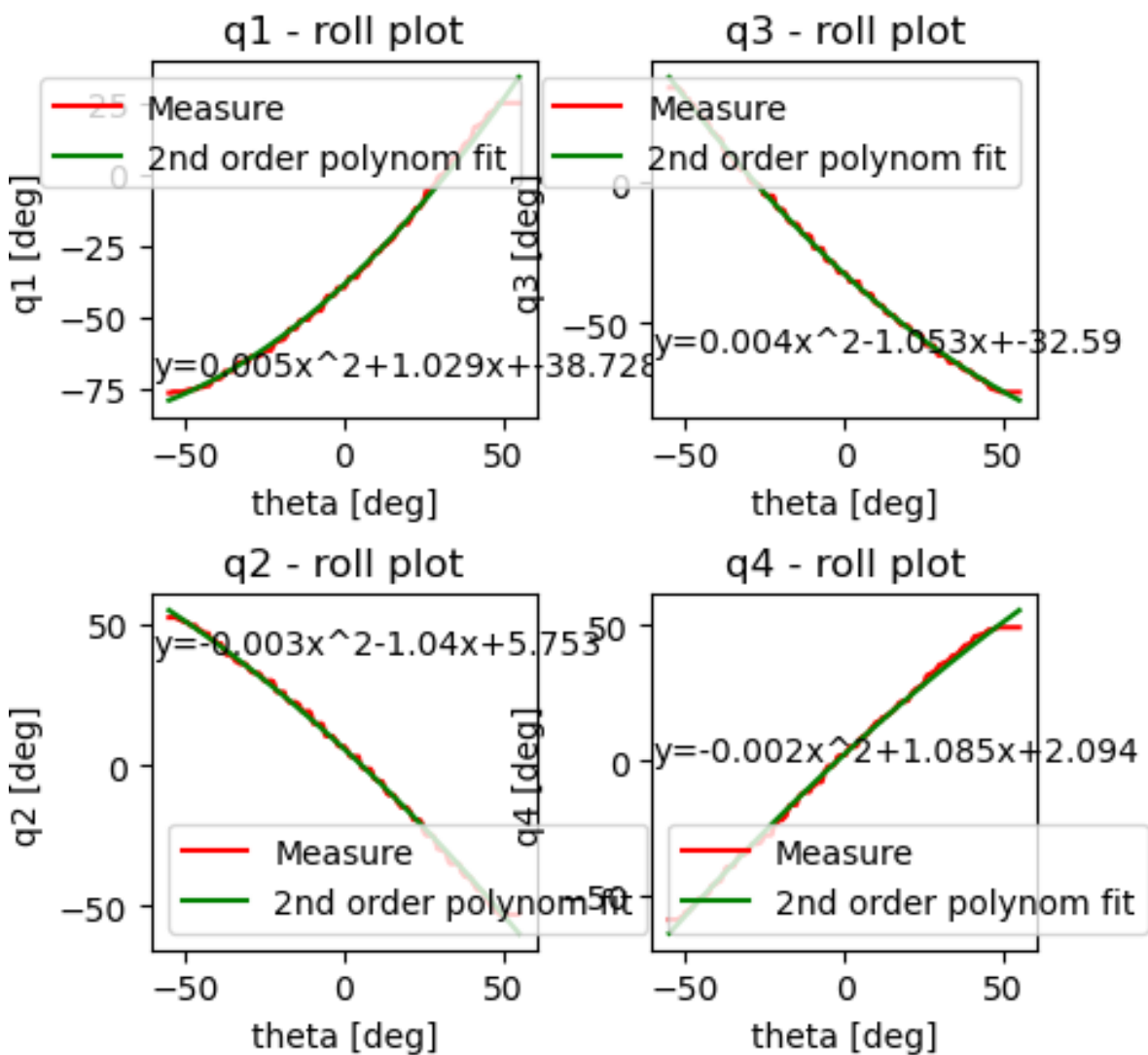


Figure 5.4: $\mathcal{F}_{\theta,i}(\theta)$ fit to measure for each q_i

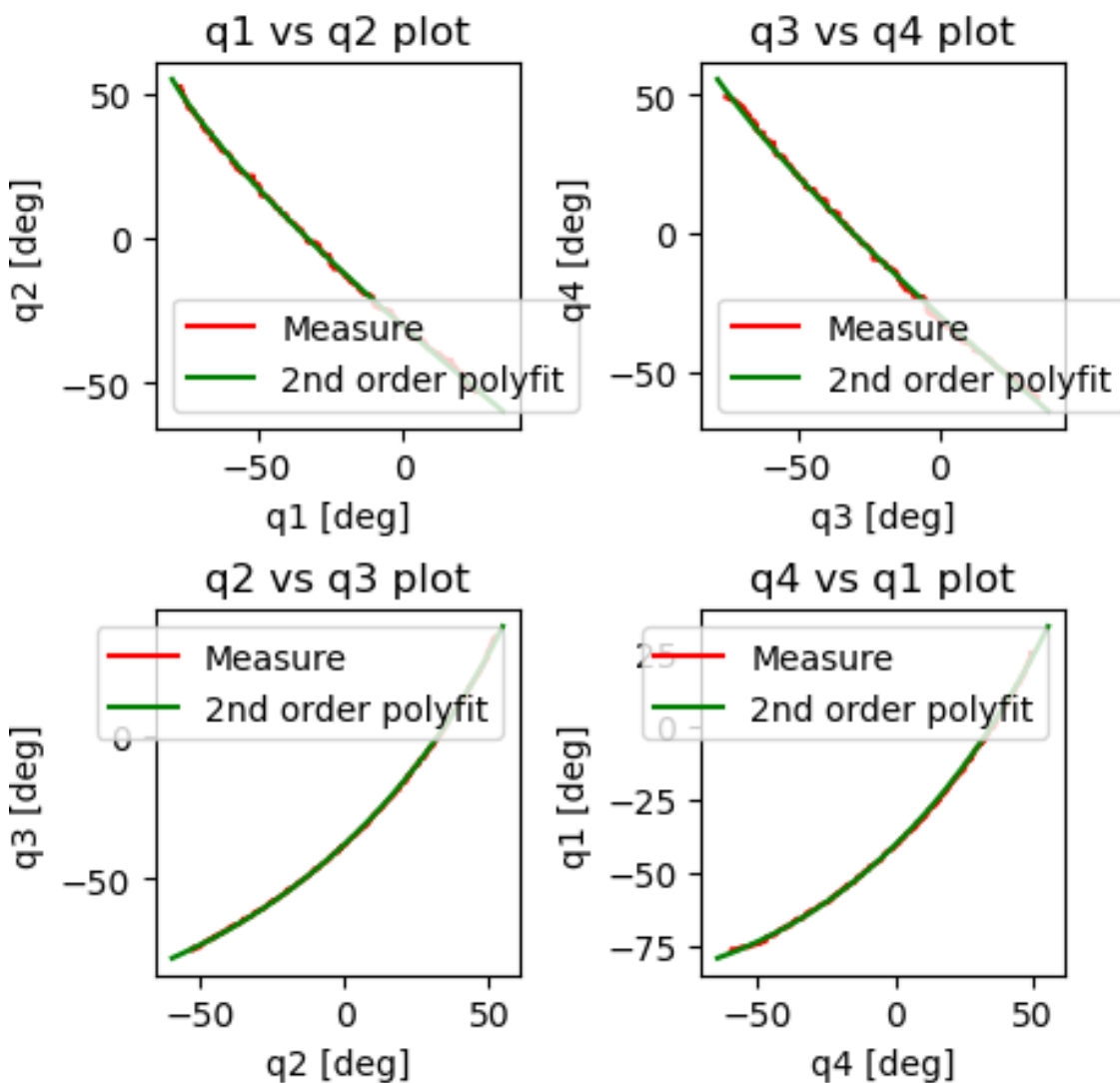
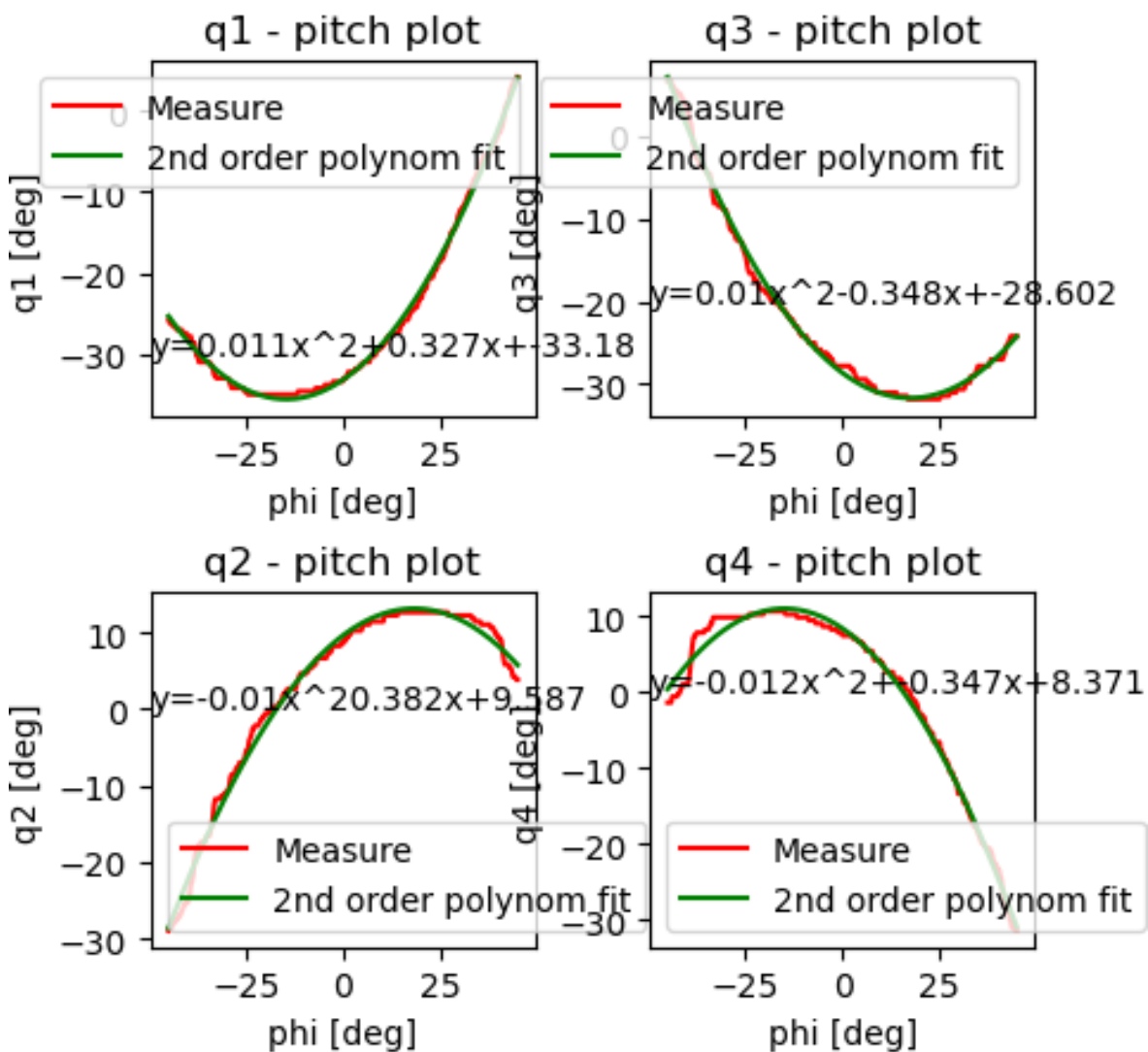


Figure 5.5: Adjacent joint vs adjacent joint measure and fit along roll axis

Figure 5.6: $\mathcal{F}_{\phi,i}(\phi)$ fit to measure for each q_i

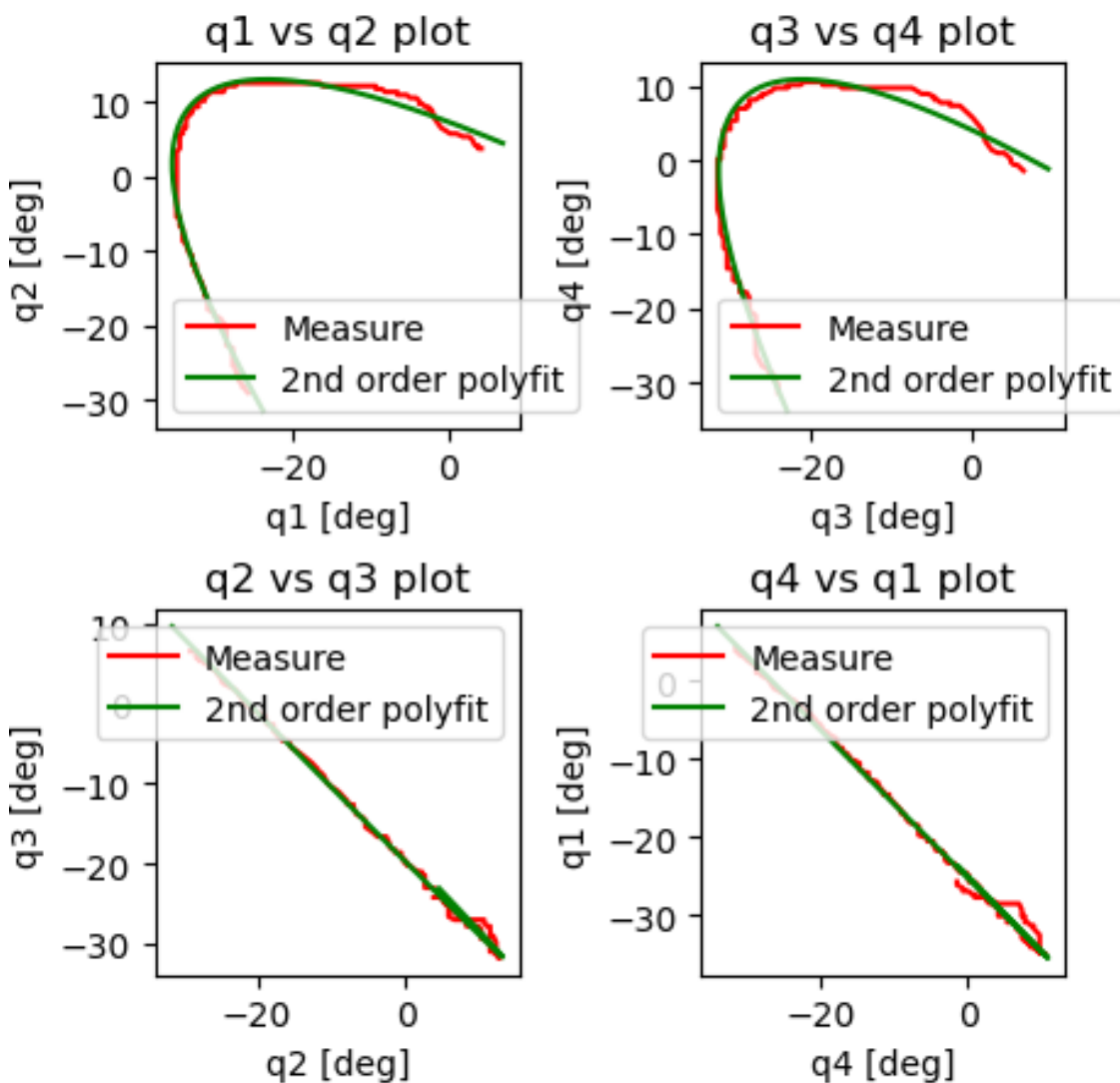
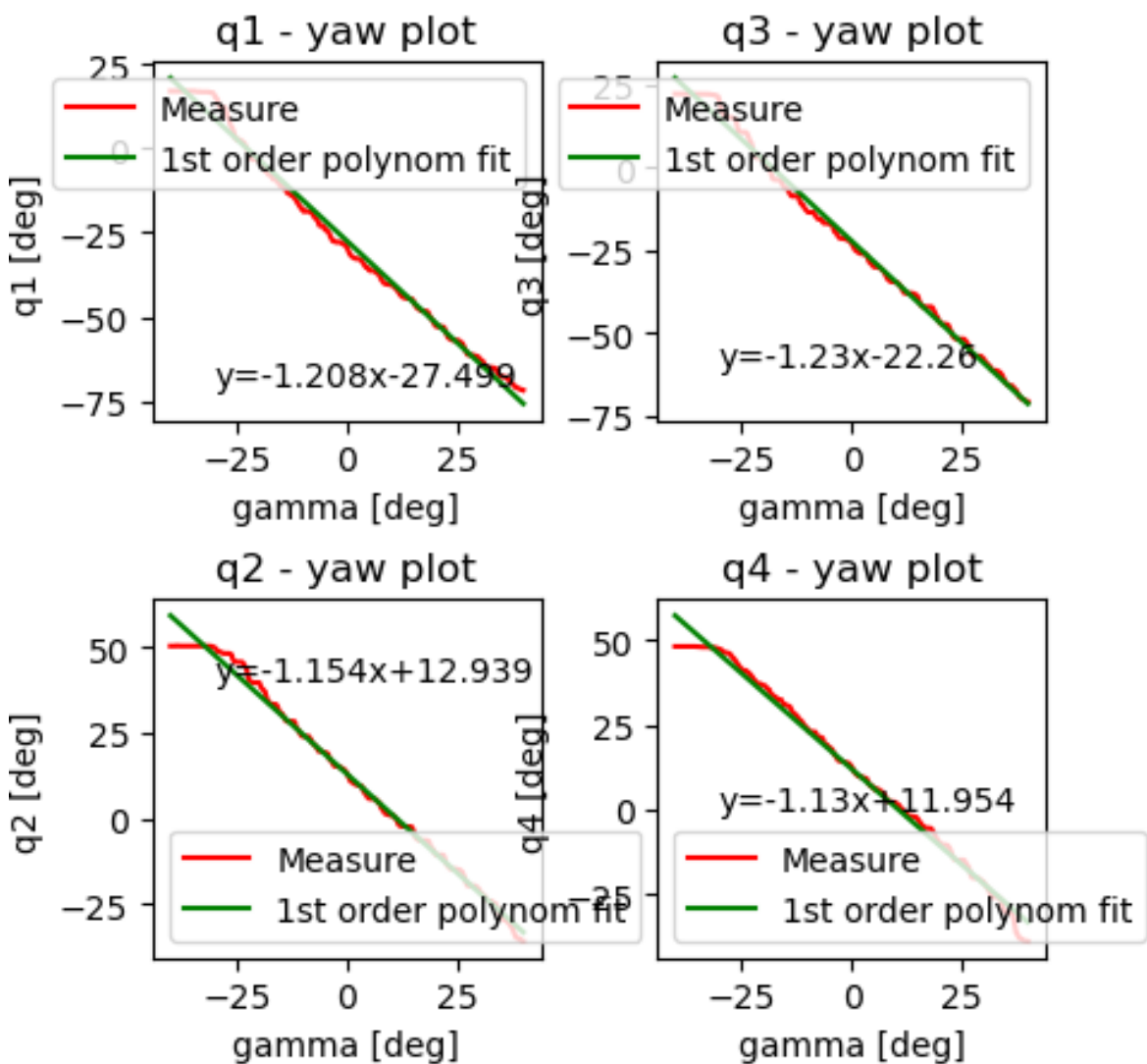


Figure 5.7: Adjacent joint vs adjacent joint measure and fit along pitch axis

Figure 5.8: $\mathcal{F}_{\gamma,i}(\gamma)$ fit to measure for each q_i

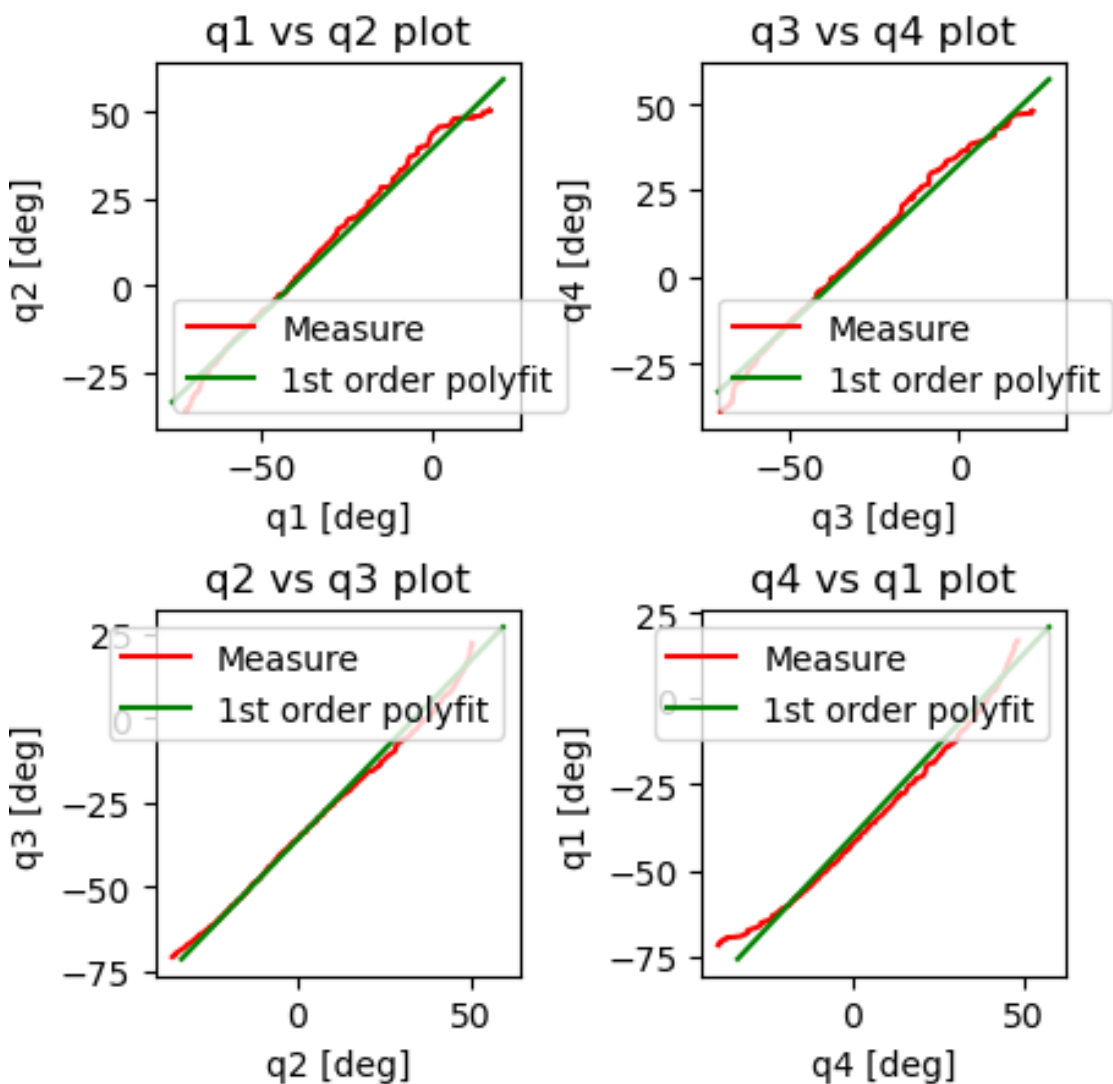


Figure 5.9: Adjacent joint vs adjacent joint measure and fit along yaw axis

6 1st project : sensing and actuation for a rotary pouch motors actuated design

6.1 Sensing

In order to control the position of the DW using rotary pouches actuation, sensors were implemented in the prototype to sense the bottom hinges angles. There are 4 sensors, for 4 bottom hinges. This was obsolete once DC-motors with absolute encoders replaced rotary pouches actuation. This part intends to show the work done.

6.1.1 Sensors selection

The sensor had to fulfill the following requirements:

- Angular measurement
- Absolute angle sensing, to avoid calibration when starting the prototype
- Bandwidth greater than 1 KHz at least, for haptic control
- Angular resolution of 0.1 deg at least
- Angular precision of 1 deg at least
- No interference between the different sensors
- Readable with an Arduino Mega2560 (3.3V or 5V)
- Easy to solder and mountable on our prototype

Considering those requirements, the Magnetic Rotary Encoder AS5048A was chosen. This sensor is based on Hall-effect. Its specifications are the following:

6.1.2 Sensing design

The design is the integration of the sensing on the platform. The aim is to place the magnet and the Hall-effect sensor on the platform in a way such that the bottom-hinges angles of the DW are sensed. The requirements were:

- No force induced, for instance friction
- Less than 0.25mm of misalignment between the AS5048 Hall-effect sensor and the magnet
- Compatible with the integration of rotary pouch actuators
- Repeatability from one usage to another

| Requirement | AS5048A specification |
|---|---|
| Angular measurement | Yes |
| Absolute angle sensing | Yes and absolute-zero is programmable |
| Bandwidth | 21.25 KHz Using I ² C communication protocol (cf part 6.1.3) |
| Angular resolution | 14-bit encoding, which makes 0.021 deg resolution |
| Precision | Maximum non-linearity is ± 0.8 deg |
| No interference between the different sensors | Yes |
| Readable with an Arduino Mega2560 | Operating voltage of 3.3V or 5V, I ² C is available |
| Easy to solder | The sensor is soldered on a PCB |
| Mountable on our prototype | Yes |

Table 3: AS5048A Specifications compared to the requirements for the sensor

Each magnet is put at the end of a holder, the holder being fixed upon a bottom-hinge. In front of the magnet is placed the Hall-effect sensor (see fig. 6.1, 7.1, 7.2 and 7.3) As the middle of the magnet is placed on the rotational axis of the bottom-hinge, in purely theoretical geometry, the magnet only rotates and doesn't shift. In practise, before hinge width characterization, the magnets shifted up to 0.75mm at extreme angles, but the Hall-effect sensor was still able to read absolute angle. After hinge characterization, shift had a maximum 0.1mm magnitude.

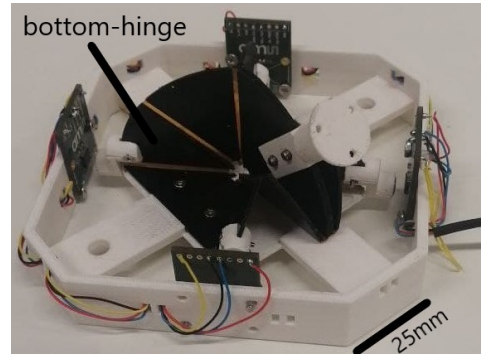


Figure 6.1: Integration of Hall-effect sensors on the platform

6.1.3 Sensors reading using I²C

I²C is the communication protocol used for reading the sensors. The maximum clock frequency is 3.4MHz. Considering the reading of 2 bytes times 4 sensors plus a time lapse between each reading, each sensor is readable at 21.25 KHz.

A strong advantage of I²C is that it can be daisy-wired, to limit the number of wires on the prototype. The wiring scheme is shown on fig. 6.6. To read the sensors, there are Arduino and MATLAB libraries. An ID tag was manually burnt on each sensor in order to select which one to read.

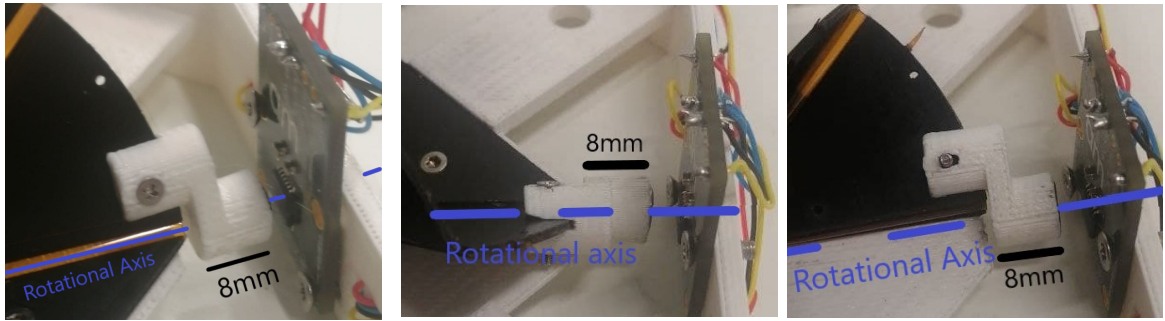


Figure 6.2: 0 degrees

Figure 6.3: -55 degrees

Figure 6.4: 35 degrees

Figure 6.5: Implemented sensing design, at different bottom-hinge angles

$$f_{reading} = \frac{f_{I^2C}}{N_{sensors} \times (L_{protocol} + L_{TimeLapse})}$$

$$f_{reading} = 21.25 \text{ KHz}$$

| |
|--|
| $f_{I^2C} = 3.4 \text{ MHz}$ $N_{sensors} = 4$ $L_{protocol} = 2 \text{ B} \times 8 = 16 \text{ bits}$ $L_{TimeLapse} = 1 \text{ B} \times 8 \text{ bits} = 8 \text{ bits}$ |
|--|

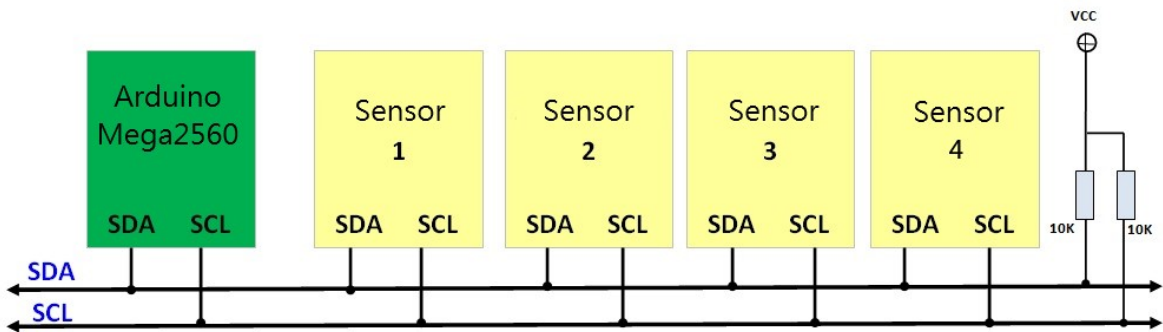


Figure 6.6: Electrical scheme of the wiring for the sensing of the first prototype

6.2 Actuation

This part will cover the exploration of pouch motors actuation. Ways to extend the range of actuation of pouch motors will be explored. Pouch motors can be fixed on joints DC motors couldn't actuate, which is a strong advantage. Eventually, the reason why this way of actuation was cancelled will be exposed.

6.2.1 Stacking pouches to propose a different type of Rotary Pouch Actuator than Adibnazai and al., 2020

Adibnazai and al., 2020 describes their mechanism this way:

The mechanism governing rotary pouch motor actuation is extremely simple: two inextensible polymer sheets are bonded to form an inflatable pouch. After this pouch is adhered to an underlying linkage, inflation creates tension in the pouch membrane that, in turn, pulls the links together, inducing rotation in the joint. The pouch can therefore be controlled in pressure, or in angle using a feedback loop⁽⁸⁾.

This mechanism is shown in fig. 6.7. Experimentally, it works for a relatively large angular range (up to 60°). But, this is not enough for actuating the Waterbomb on its full range, and also it may not be robust enough to be in interaction with humans - especially VR players.

As an alternative solution, what was explored in the project is the following idea. Instead of using pouch motors as a tension generator, pouches are pushing the tiles in order to create a torque. To reach a sufficient range of motion, another innovation brought in this project was to stack pouches together inside a joint in order to increase the range. With 4 stacked pouches, the joint is able to reach a 180° angle, see fig. 6.7. The idea of stacking pouches was already implemented using fluids in the Elastomeric Donut HASEL Actuator⁽¹²⁾ of Rothemund and al., 2020.

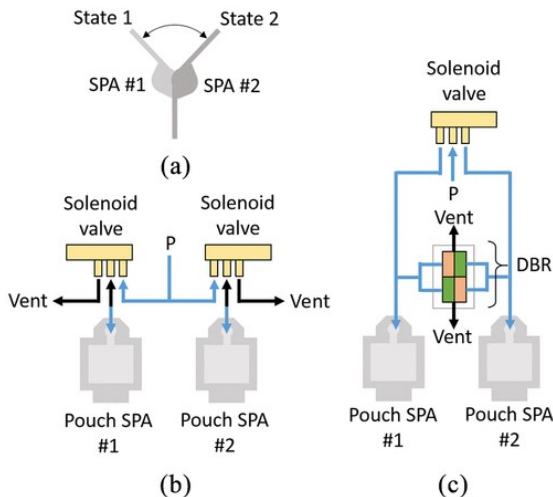


Figure 6.7: Adibnazai antagonistic pouch⁽⁹⁾

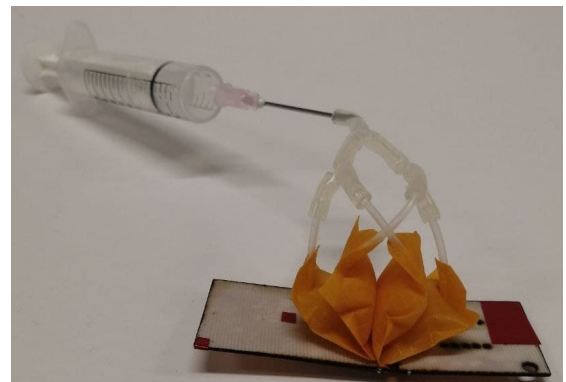


Figure 6.8: Proposition for an origami-based structure single joint, actuated by fully-inflated stacked rotational pouch actuators, reaching 180°

6.2.2 Pouch motors are a good option for origami-based VR controller

Pouch-motors can be fixed on the mid-hinge of the DW, that DC-motor cannot access. This makes the control much easier, as the following 1-to-1 function can be written:

$$\vec{d}(\phi, \theta, \gamma) = \vec{\mathcal{F}}(\vec{\alpha}) \quad (6.1)$$

Where:

$\vec{\alpha}$ is the 4x1 vector of mid-hinges angles

$\vec{\mathcal{F}}$ is a $\mathcal{R}^3 \rightarrow \mathcal{R}^4$ 1-to-1 function

\vec{d} is the orientation of the joystick expressed in Euler angles

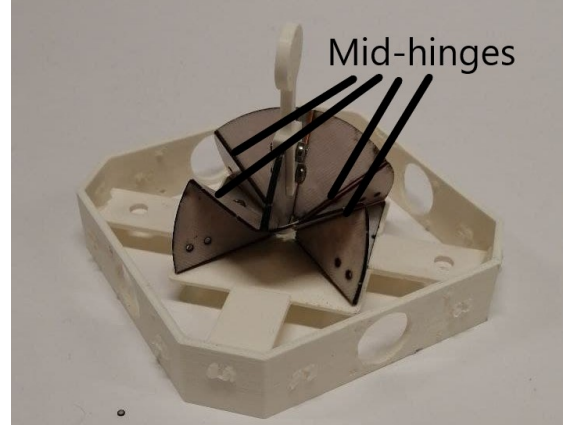


Figure 6.9: Position of the mid-hinges on the DW

6.2.3 Why Pouch motors were not implemented in DW ?

At the moment, there is not enough characterization and modeling for rotary pushing pouch-actuators to implement position control. A main difficulty using pouch motors is to control the position, the stiffness and the damping factor. The only input that is given to the pouch is pressure.

This project is an opening for research in rotary pushing pouch-actuators.

7 2nd project: DC-motor integration and control

This section covers the selection of the motor, its integration on the haptic origami-based platform and its different types of control.

7.1 Motor selection

The selected motor should fit the following requirements:

- Integrating or compatible with an absolute position encoder
- A maximum torque under 0.3 [N.m] to avoid breaking the DW
- Mechanically integrable on the platform
- Not too expensive
- A reasonable cutoff frequency to control the motor

The **dynamixel XL330-M077** was selected, because it presented the following specifications:

- Integrated MCU, integrating position control operating mode and current-based position control mode, with gives a very high frequency for
- Integrated encoder 4096 [pulse/rev]
- Maximum torque of 0.215 [N.m]
- Adapted to the platform as light-weight (18g) and at the platform's dimensions
- Costs 20 US\$
- Daisy wiring and unique ID, which makes easy to control every of them with a PC
- Settable range of positions, which avoids breaking the DW

7.2 Design

The same principle than for the sensing was applied to link the rotational bottom-hinges of the DW to a static element on the platform. A 3D printed part, named the holder, links the motor to the DW. The motor is screwed on the platform, such that its center is aligned with the rotation axis of the bottom-hinges.

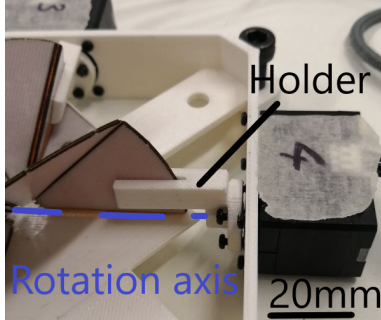


Figure 7.1: 0 degrees

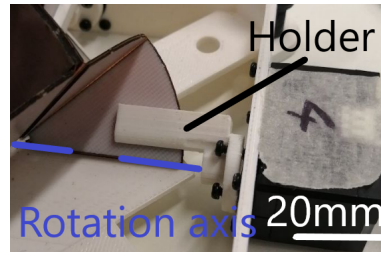


Figure 7.2: -30 degrees

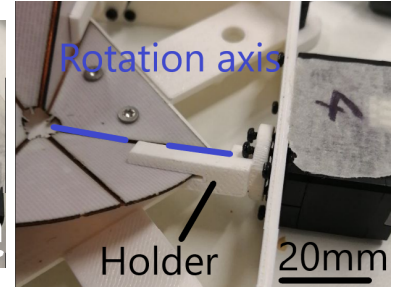


Figure 7.3: 60 degrees

Figure 7.4: Implemented DC-motor actuation design, at different bottom-hinge angles

7.3 Hardware and software setups

The section will cover the pure low-level parts of the control, such as libraries and electronic setup. Two setups are used, one for exploration and one for performance.

EXPLORATION SETUP

The first setup uses U2D2 and Python Dynamixel SDK, and is very convenient to try new types and control and talking measurements. Still, performances are low due to the PySerial library: this setup takes around 15ms to send to one motor an instruction. As the Dynamixel SDK API was not sufficient, a whole API was developed on the base of the Dynamixel API during this project. The baud rate used is 4MBps. The setup is shown on fig. 7.5.



Figure 7.5: Exploration hardware setup

PERFORMANCES SETUP

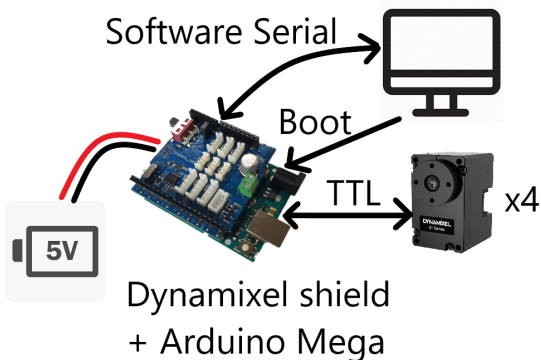


Figure 7.6: Performance hardware setup

This setup uses Dynamixel Shield and Arduino Dynamixel SDK. It present higher performances, such as 3.7ms to send one motor an instruction. Thought, debugging is harder on this setup. Beware not to change the Baud rate of the TTL communication above 2 Mbps, otherwise Arduino boards won't be able to manage it. The setup is shown on fig. 7.6. A software Serial port have to be used for the communication with the computer, because the hardware serial port is already used for the TTL communication with the motors.

7.4 Control in position

The motors have embedded PID controllers, and the forward kinematic model allows us to find $\vec{q} = \vec{\mathcal{F}} \begin{pmatrix} \theta \\ \phi \\ \gamma \end{pmatrix}$. Yet, the control in position is implemented this way:

1. Set the 4 PID controller values at start
- While controlling in position:
 2. Select a target \vec{d} for the joystick axis
 3. Compute $\vec{q} = \vec{\mathcal{F}}(\vec{d})$
 4. Feed \vec{q} to the 4 PID controllers
 5. Wait for next iteration

8 Discussion

8.1 Design improvement advantages

Double-Waterbomb presents an opportunity to create a compliant and actionable spherical joint. Having a method to get a sample standing up straight is an advantage for this robogami: for many usages as a video game controller, it can be useful to have a centered rest position and a natural stiffness such that the DW gets back to it. Though, the method is based on a joint width characterization for specific widths of Kapton and FR4. To know the best joint width for any Kapton/FR4 width pair and therefore be able to produce better any type of robogami, a larger study could be made, to fit a model or to give a look-up table.

Another advantage of this joint-width study would be to avoid having unconstrained parasites movements around the joint axis, and then better precision using robogamis.

Eventually, one of the issues of the DW is that it can get stuck into singularities. The natural stiffness brought by a $125\mu\text{m}$ Kapton avoid getting into those singularities. Having a 4 bottom-hinges controlled DW also avoids getting into singularities.

8.2 A simple model for high performances and popular use

In this report is proposed a polynom-based kinematic model. Its strength is that it is extremely simple for such a closed loop kinematic structure.

This is an opportunity for embedded systems implementation, because required processing power becomes very low. It means higher cutoff frequencies for the controller and lower requirements for the processors. Polynoms can be derived easily, which is an advantage for feed-forward control systems.

People use what's easy to use. If such a model exists, this is an opening for Double-Waterbomb usage in the industry. One more advantage is added to its already existing light-weight, low-cost and easy-to-manufacture properties. Eventually, the model is only angle-based: it means that the numerical values computed in this project are valid for any DW made out of circular or squared Waterbombs.

Though, the inverse kinematic model still needs to be computed. This part of the project was not in the initial scope, but as a model was needed to control the joystick, this one was empirically found. As a matter of fact, it fits extremely well the measurements. Using numeric solvers and the kinematic model, the inverse kinematic model could be found easily. Inverse kinematic model is required to implement haptic control.

A innovative way to get a model of the DW would be to use Bruder's Koopman operator based system identification method⁽¹³⁾. It is fit for soft-robots and data is easy to collect with encoders, which opens the door for data-driven system identification.

8.3 Using Pouch motors asymmetry to implement haptics

Stacked rotary pouch motors are an interesting way to create structures with a natural spring and damper behavior. For a haptic controller, this is an opportunity to react instantly to the user movements by generating a pre-defined "authorized" motion of range. The "natural" sensation of touching a naturally compliant air pouch is a strong advantage for haptic, compared to DC motors for instance.

The rotational pouch motors have an asymmetric actuation, this is why a joint is typically actuated by two antagonistic pouches, like two antagonistic muscles (seen in fig. 6.7). The separation of the two rotational directions is an opportunity to dynamically create naturally compliant and damping walls. If only one pouch is inflated, the joint will be free in a certain range of motion away from the pouch, and constrained as it pushed against the pouch (fig. 8.4).

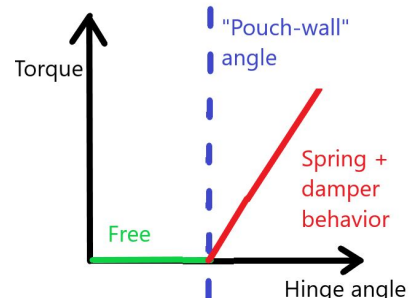


Figure 8.1: Modelization of "pouch-wall"

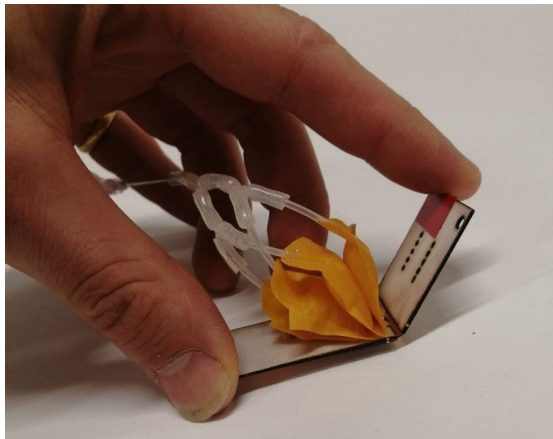


Figure 8.2: With no torque applied

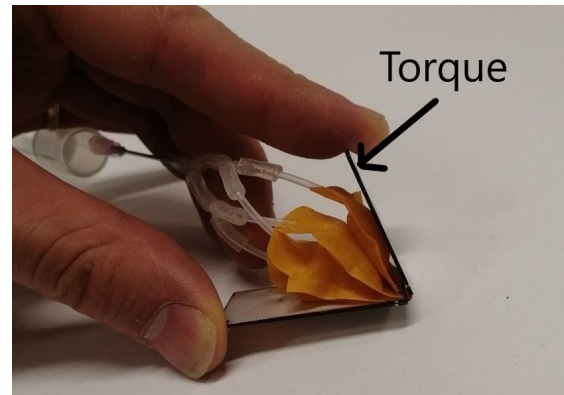


Figure 8.3: With a torque applied

Figure 8.4: Origami-based structure single joint, actuated by stacked rotational pouch actuators

Applied to a VR haptics controller, this would allow the controller to define dynamically a range of motion in which the user can move. For instance, let's suppose that a Waterbomb is used as a VR haptic controller, the user controlling roll, pitch and yaw. Let's say that in the virtual world, there is a wall in front of the user. The user shouldn't be able to move his hand forward. Then, the "front pouches" of the controller would inflate, preventing the user to move forward but letting it perfectly free otherwise.

Compared to a virtual wall controller implemented on a DC motor, the advantages of the pouch motor is that the sensation for the user is very smooth as is it air-driven. Compliance and damping factors could be changed using a less-compressible fluid than air. As the wall is real, not virtual, the cutoff frequency of the pouch-wall is infinite. It avoids issues triggered by haptic control using DC motor, such that fine-tuning of the cutoff frequency to make a trade-off between compliance and damping, or vibrations due to sensing noise.

8.4 DC-motor control position is accurate, but not adapted to haptic

The implemented control on this project is rather basic, position control using PID controllers. The DW is finely actuated, which is a step forward in DW control. Still, to get better position control, more performant control methods could be implemented, for instance Model Predictive Control.

Though, it is an open-loop control system with regards to the user, and it is not adapted to haptic control. Once the inverse kinematic model is known, control in torque would open the door to haptic control.

In order to get the best performances, the frequency at which the PID is given a new \vec{q} must be above 60 Hz. But, to avoid having the DW shaking, the motors must all be actuated at the same time. Arduino Mega gives satisfying results, but to use DW as a high precision tool, a better hardware implementation with a higher refresh frequency would be needed.

9 Conclusion

The final aim of this project is to create an origami-based VR controller, pouch-actuated. Even though this goal hasn't been reached yet, encouraging steps forward have been made this semester.

The State-of-the-Art of the Double-Waterbomb robogami have been updated. A stiffness characterization has been added, and several issues with design have been solved.

A kinematic model is proposed for the DW. However, this model still needs to be properly tested, even if it seems very accurate from the first observations. The inverse kinematic model is still needed to implement closed-loop control - such as haptic control. Though, having a light kinematic model may help to find an inverse kinematic model.

The DW is now integrated on a platform, driven by DC-motors and encoders. If this is not the final way of actuating the DW, this platform is a good playground to test control methods, models, stiffness, many things that are better to test on an easy-to-control platform than with challenging pouch actuators.

Pouch actuators have been explored, replacing pulling pouches by pushing stacked pouches. Those results, crossed with the kinematic model, allow the upcoming projects to control the DW with pouch actuation on its bottom-hinges. Pouch-compatible sensing is already designed, implemented and tested. Though, a folding issue needs to be tackled first. Also, a model is required to control the pouches, which may be challenging.

Eventually, thanks to Bruno, a brilliant VE interface is now available to test the controllers.

As a conclusion, I would like to thank Prof. J. Paik for the opportunity she gave me to perform this semester project. I would also like to thank Mustafa Mete for his encouraging management, his good advices and his constant support.

10 Bibliography

References

- [1] D. J. Balkcom and M. T. Mason, “Robotic origami folding,” *The International Journal of Robotics Research*, vol. 27, no. 5, pp. 613–627, 2008.
- [2] C. D. Onal, R. J. Wood, and D. Rus, “An origami-inspired approach to worm robots,” *IEEE/ASME Transactions on Mechatronics*, vol. 18, no. 2, pp. 430–438, 2013.
- [3] H. Suzuki and R. J. Wood, “Origami-inspired miniature manipulator for teleoperated microsurgery,” *Nature Machine Intelligence*, vol. 2, no. 8, pp. 437–446, 2020.
- [4] S. Li, J. J. Stampfli, H. J. Xu, E. Malkin, E. V. Diaz, D. Rus, and R. J. Wood, “A vacuum-driven origami “magic-ball” soft gripper,” in *2019 International Conference on Robotics and Automation (ICRA)*, pp. 7401–7408, IEEE, 2019.
- [5] D. Rus and C. Sung, “Spotlight on origami robots,” *Science Robotics*, vol. 3, no. 15, 2018.
- [6] M. T. Tolley, S. M. Felton, S. Miyashita, D. Aukes, D. Rus, and R. J. Wood, “Self-folding origami: shape memory composites activated by uniform heating,” *Smart Materials and Structures*, vol. 23, no. 9, p. 094006, 2014.
- [7] D. Rus and M. T. Tolley, “Design, fabrication and control of origami robots,” *Nature Reviews Materials*, vol. 3, no. 6, pp. 101–112, 2018.
- [8] I. Adibnazari, B. J. Jeon, Y.-L. Park, and M. T. Tolley, “Versatile rotary actuators for small-scale robotic systems,” in *2020 3rd IEEE International Conference on Soft Robotics (RoboSoft)*, pp. 873–878, 2020.
- [9] M. A. Robertson, O. C. Kara, and J. Paik, “Soft pneumatic actuator-driven origami-inspired modular robotic “pneumagami”,” *The International Journal of Robotics Research*, vol. 40, no. 1, pp. 72–85, 2021.
- [10] H. A. Sonar, A. P. Gerratt, S. P. Lacour, and J. Paik, “Closed-loop haptic feedback control using a self-sensing soft pneumatic actuator skin,” *Soft robotics*, vol. 7, no. 1, pp. 22–29, 2020.
- [11] J.-L. Huang, Z. Zhakypov, H. Sonar, and J. Paik, “A reconfigurable interactive interface for controlling robotic origami in virtual environments,” *The International Journal of Robotics Research*, vol. 37, no. 6, pp. 629–647, 2018.

- [12] P. Rothemund, N. Kellaris, S. K. Mitchell, E. Acome, and C. Keplinger, “Hasel artificial muscles for a new generation of lifelike robots—recent progress and future opportunities,” *Advanced Materials*, p. 2003375, 2020.
- [13] D. Bruder, B. Gillespie, C. D. Remy, and R. Vasudevan, “Modeling and control of soft robots using the koopman operator and model predictive control,” *CoRR*, vol. abs/1902.02827, 2019.